



# **Time-Reversal Based Range Extension Technique for Ultra-wideband (UWB) Sensors and Applications in Tactical Communications and Networking**

Technical Report (Quarterly)

to

US Office of Naval Research

875 North Randolph Street

Arlington, VA 22203-1995

for

Grant # N00014-07-1-0529

Prepared by

Robert C. Qiu

**(Principal Investigator)**

together with

(Contributing Researchers at Wireless Networking Systems Lab)

Nan (Terry) Guo

Yu Song

Peng (Peter) Zhang

Zhen (Edward) Hu

**October 16, 2009**

Department of Electrical and Computer Engineering

Center for Manufacturing Research

Tennessee Technological University

Cookeville, TN 38505

# **20100125634**

## Acknowledgment

This work has been improved by discussions with S. K. Das (ONR), B. M. Sadler (ARL), R. Ulman (ARO), and L. Lunardi (formerly with NSF). K. Currie (CMR, TTU) has provided a lot of support for this project. S. Parkc (ECE, TTU) has supported our research in different ways. We also want to thank P. K. Rajan for helpful discussions.

REPORT DOCUMENTATION PAGE					Form Approved OMB No. 0704-0188	
<p>The public reporting burden for this collection of information is estimated to average 1 hour per response, including the time for reviewing instructions, searching existing data sources, gathering and maintaining the data needed, and completing and reviewing the collection of information. Send comments regarding this burden estimate or any other aspect of this collection of information, including suggestions for reducing the burden, to Department of Defense, Washington Headquarters Services, Directorate for Information Operations and Reports (0704-0188), 1215 Jefferson Davis Highway, Suite 1204, Arlington, VA 22202-4302. Respondents should be aware that notwithstanding any other provision of law, no person shall be subject to any penalty for failing to comply with a collection of information if it does not display a currently valid OMB control number.</p> <p><b>PLEASE DO NOT RETURN YOUR FORM TO THE ABOVE ADDRESS.</b></p>						
1. REPORT DATE (DD-MM-YYYY) 16-07-2009		2. REPORT TYPE Technical Report (Quarterly)			3. DATES COVERED (From - To) July 16, 2009 -- October, 2009	
4. TITLE AND SUBTITLE Time-Reversal Based Range Extension Technique for Ultra-wideband (UWB) Sensors and Applications in Tactical Communications and Networking				5a. CONTRACT NUMBER		
				5b. GRANT NUMBER N00014-07-1-0529		
				5c. PROGRAM ELEMENT NUMBER		
6. AUTHOR(S) Qiu, Robert C.; Guo, Nan; Song, Yu; Zhang, Peng; Hu, Zhen				5d. PROJECT NUMBER		
				5e. TASK NUMBER		
				5f. WORK UNIT NUMBER		
7. PERFORMING ORGANIZATION NAME(S) AND ADDRESS(ES) Tennessee Technological University 115 W. 10th Street Cookeville, TN 38501				8. PERFORMING ORGANIZATION REPORT NUMBER		
9. SPONSORING/MONITORING AGENCY NAME(S) AND ADDRESS(ES) US Office of Naval Research 875 North Randolph Street Arlington, VA 22203-1995				10. SPONSOR/MONITOR'S ACRONYM(S) ONR		
				11. SPONSOR/MONITOR'S REPORT NUMBER(S) 07PR05074-00		
12. DISTRIBUTION/AVAILABILITY STATEMENT release for public distribution.						
13. SUPPLEMENTARY NOTES						
14. ABSTRACT In this quarter our development work has been emphasized on expanding functionalities. In system development aspect, details in 2x1 MISO and wideband coherent receiver design are reported. In addition, some related theoretical work done in this period is reported too. The technologies and experience gained from this project are benefiting and will continue to drive our researches in UWB MIMO, waveform diversity, wideband RF frontend, and Wideband digital beamforming.						
15. SUBJECT TERMS UWB, testbed, time reversal, range extension, sensors, multi-GHz wideband, cognitive radio						
16. SECURITY CLASSIFICATION OF:			17. LIMITATION OF ABSTRACT  UU	18. NUMBER OF PAGES  24	19a. NAME OF RESPONSIBLE PERSON Francis Otuonye	
a. REPORT  U	b. ABSTRACT  U	c. THIS PAGE  U			19b. TELEPHONE NUMBER (Include area code) 931-372-3374	

REPORT OF INVENTIONS AND SUBCONTRACTS  
(Pursuant to "Patent Rights" Contract Clause) (See Instructions on back)

Form Approved  
OMB No. 9000-0095  
Expires Jan 31, 2008

The public reporting burden for this collection of information is estimated to average 1 hour per response, including the time for reviewing instructions, searching existing data sources, gathering and maintaining the data needed, and completing and reviewing the collection of information. Send comments regarding this burden estimate or any other aspect of this collection of information, including suggestions for reducing the burden, to the Department of Defense, Executive Services Directorate (9000-0095). Respondents should be aware that notwithstanding any other provision of law, no person shall be subject to any penalty for failing to comply with a collection of information if it does not display a currently valid OMB control number.

PLEASE DO NOT RETURN YOUR COMPLETED FORM TO THE ABOVE ORGANIZATION. RETURN COMPLETED FORM TO THE CONTRACTING OFFICER.

1.a. NAME OF CONTRACTOR/SUBCONTRACTOR Tennessee Technological University	c. CONTRACT NUMBER N00014-07-1-0529	2.a. NAME OF GOVERNMENT PRIME CONTRACTOR US Office of Naval Research	c. CONTRACT NUMBER N00014-07-1-0529	3. TYPE OF REPORT (X one) <input checked="" type="checkbox"/> a. INTERIM <input type="checkbox"/> b. FINAL
b. ADDRESS (Include ZIP Code) 115 W. 10th Street Cookeville, TN 38501	d. AWARD DATE (YYYYMMDD) 20070116	b. ADDRESS (Include ZIP Code) 875 North Randolph Street Arlington, VA 22203-1995	d. AWARD DATE (YYYYMMDD) 20070416	4. REPORTING PERIOD (YYYYMMDD) a. FROM 20090716 b. TO 20091016

SECTION I - SUBJECT INVENTIONS

5. "SUBJECT INVENTIONS" REQUIRED TO BE REPORTED BY CONTRACTOR/SUBCONTRACTOR (If "None," so state)					
NAME(S) OF INVENTOR(S) (Last, First, Middle Initial)	TITLE OF INVENTION(S) b.	DISCLOSURE NUMBER, PATENT APPLICATION SERIAL NUMBER OR PATENT NUMBER c.	ELECTION TO FILE PATENT APPLICATIONS (X)		CONFIRMATORY INSTRUMENT OR ASSIGNMENT FORWARDED TO CONTRACTING OFFICER (X) a.
			(1) UNITED STATES (a) YES (b) NO	(2) FOREIGN (a) YES (b) NO	
None					

f. EMPLOYER OF INVENTOR(S) NOT EMPLOYED BY CONTRACTOR/SUBCONTRACTOR		g. ELECTED FOREIGN COUNTRIES IN WHICH A PATENT APPLICATION WILL BE FILED	
(1) (a) NAME OF INVENTOR (Last, First, Middle Initial)	(2) (a) NAME OF INVENTOR (Last, First, Middle Initial)	(2) FOREIGN COUNTRIES OF PATENT APPLICATION	
(b) NAME OF EMPLOYER			
(c) ADDRESS OF EMPLOYER (Include ZIP Code)	(c) ADDRESS OF EMPLOYER (Include ZIP Code)		

SECTION II - SUBCONTRACTS (Containing a "Patent Rights" clause)

6. SUBCONTRACTS AWARDED BY CONTRACTOR/SUBCONTRACTOR (If "None," so state)							
NAME OF SUBCONTRACTOR(S) a.	ADDRESS (Include ZIP Code) b.	SUBCONTRACT NUMBER(S) c.	FAR "PATENT RIGHTS" d.		DESCRIPTION OF WORK TO BE PERFORMED UNDER SUBCONTRACT(S) a.	SUBCONTRACT DATES (YYYYMMDD) f.	
			(1) CLAUSE NUMBER	(2) DATE (YYYYMM)		(1) AWARD	(2) ESTIMATED COMPLETION
None							

SECTION III - CERTIFICATION

7. CERTIFICATION OF REPORT BY CONTRACTOR/SUBCONTRACTOR (Not required if: (X as appropriate))			SMALL BUSINESS or	NONPROFIT ORGANIZATION
I certify that the reporting party has procedures for prompt identification and timely disclosure of "Subject Inventions," that such procedures have been followed and that all "Subject Inventions" have been reported.				
a. NAME OF AUTHORIZED CONTRACTOR/SUBCONTRACTOR OFFICIAL (Last, First, Middle Initial) Otuonye, Francis	b. TITLE Associate Vice President	c. SIGNATURE N/A	d. DATE SIGNED	

## Executive Summary

In this quarter our development work has been emphasized on expanding functionalities. In system development aspect, details in 2x1 MISO and wideband coherent receiver are reported. In addition, some related theoretical work done in this period is reported too. The technologies and experience gained from this project are benefiting and will continue to drive our researches in UWB MIMO, waveform diversity, wideband RF frontend, and Wideband digital beamforming.

# Contents

<b>I</b>	<b>System Development</b>	<b>1</b>
1	System Improvement Work	3
1.1	Experimental Results of 2-by-1 Ultra-Wideband MISO Radio Testbed . . . . .	3
1.1.1	Experiment Results . . . . .	3
1.2	Real Time Waveform Loading . . . . .	4
2	Wideband Multichannel Coherent Receiver Design	9
2.1	Background . . . . .	9
2.2	Overall Architecture . . . . .	9
2.3	Analog Frontend (Tuner) . . . . .	9
2.4	Automatic Gain Control (AGC) . . . . .	10
2.5	Digitizer Architecture . . . . .	11
2.6	Sundance 4 channels digitizer system with FPGA processing . . . . .	11
3	Theoretical Work	15
3.1	Wideband Waveform Optimization for Multiple Input Single Output Cognitive Radio with Practical Consideration . . . . .	15
3.1.1	Introduction . . . . .	15
3.1.2	Wideband Waveform Optimization Using Cauchy–Schwarz Inequality-based Iterative Method	16
3.1.3	Wideband Waveform Optimization Using SDP-based Iterative method . . . . .	21
3.1.4	Waveform Design with Practical Considerations . . . . .	23

3.1.5	Numerical Results . . . . .	25
3.1.6	Discussion . . . . .	28

**Part I**

**System Development**

## Chapter 1

# System Improvement Work

### 1.1 Experimental Results of 2-by-1 Ultra-Wideband MISO Radio Testbed

In the last quarter, A 2-by-1 MISO system has been built, the system was tested and experimental results are achieved.

Figure 1.1 shows the system architecture, where there are two transmit channels at transmitter side and only one receive channel at receiver side. As the most powerful device for parallel signal processing, FPGA plays a critical role in the system, all waveform algorithms will be implemented in FPGA. The two digital outputs with both I and Q phase from the FPGA board will be sent to two identical dual channel digital-to-analog converter (DAC) boards, which are capable of 1Gsamples/sec and 14 bits of precision. The receiver is energy detection based as a low-complexity reception technique which eliminates the need for channel estimation and precise synchronization.

The receiver currently being used is energy detection based. In this experiment, we only aim to observe the peak detected with the benefited MISO system versus SISO system, so the modulated data will not be transmitted from FPGA, just the time reversal waveforms be transmitted from the dual core D/A converter, because each core need to handle one channel, so the waveforms will be only I-phase based or Q-phase based, this will inevitably cause the in-balance of wireless channel information.

#### 1.1.1 Experiment Results

The main challenge is to make sure the synchronization of the two different hardware chains, which means the waveform should be generated from the two transmitter antennas at the same time. In reality, this synchronization is extremely hard to synchronize if the time reversal waveforms are got from time domain.

So the experiment is to verify the MISO UWB testbed through measuring the channel impulse response (CIR) in frequency domain and using time reversal waveforms [1, 2]. The system configuration is like Fig.1 described in [1], where a set of measurements has been conducted in a lab/office area which is a typical indoor environment with chairs, desks, book shelves and equipments. Antennas used in the testbed are omni-directional ones and the height of both transmitter and receiver antennas are set to 1.5 meters. The distance between transmitter and receiver is 5 meters, and distance between two transmitter antennas are 0.8 meters. A vector network analyzer (VNA) sweeps a frequency with the range from 3.5GHz to 4.5GHz with 1 MHz resolution. Figure 1.2 shows channel 1's transfer

function and the corresponding baseband CIR. Figure 1.3 shows channel 2's transfer function and the corresponding baseband CIR. Time reversal waveforms are exploited as the transmitted signals. The received waveforms after the RF board are shown in Figure 1.4 captured by the Tektronix DPO72004 oscilloscope. It's easily observed that the peak amplitude of the 2-by-1 MISO system is almost doubled than the counter-part of the SISO system, which means the energy gain is about 3dB. The excellent consistency between the analytical results and the experimental result shows the testbed works properly.

## 1.2 Real Time Waveform Loading

Waveform loading from PC to FPGA has been developed and implemented, it enables the testbed to change transmit waveforms at run-time.

This waveform loading functions comes from the requirement of wideband beam-forming design and implementation, where filtering is a key function in digital design and the filter coefficients need to be updated frequently, so the real-time waveform loading from PC computer to digital unit FPGA becomes necessary.

The communicate between the FPGA chip and PC computer is by USB cable and UART protocol. The FPGA board we are using in the testbed's transmitter side is Xilinx Virtex-5 ML550 board, it bears a USB connector and a USB-to-UART conversion chip on board, the architecture is shown as Figure 1.5, where the chip used is Cypress CP2102, a very popular USB-to-UART chip. The CP2102 is a highly-integrated USB-to-UART Bridge Controller providing a simple solution for updating RS-232 designs to USB using a minimum of components and PCB space. The CP2102 includes a USB 2.0 full-speed function controller, USB transceiver, oscillator, EEPROM, and asynchronous serial data bus (UART) with full modem control signals.

The Universal Asynchronous Receiver Transmitter (UART) is the most widely used serial data communication circuit ever, it is a serial communication protocol, only 2 wires are need to to establish the communication link. UARTs allow full duplex communication over serial communication links as RS232. The basic functions of a UART are a microprocessor interface, double buffering of transmitter data, frame generation, parity generation, parallel to serial conversion, double buffering of receiver data, parity checking, serial to parallel conversion. The frame format of used by UARTs is a low start bit, 5-8 data bits, optional parity bit, and 1 or 2 stop bits. The frame format for data transmitted/received by a UART is given in Figure 1.6. It consists of a high idle state of the line. A character is from 5-8 data bits. The start bit is Low and the single stop bit is High.

On the computer side, there is a client software used to generate the frame format and transmit the data via one of the four Com port on the computer. First the driver for CP2102 need to be installed on computer, it makes a USB port as a virtual COM port, so to the computer side, it communicates with FPGA via COM port, to FPGA board side, it communicate with computer via USB port, then it convert the USB signal to UART signal. Then the FPGA will receive UART signal from computer and decode it to the original waveform information by FPGA processing.

Our main work is FPGA coding for receiving the UART signal and process it. As the frame structure shows, a character is from 5-8 bits, we are currently using 8 bits. The UART architecture in our design is shown as Figure 1.7, it consist three main functional blocks: Baud rate generator, receiver and transmitter. the baud rate is set to 57600.

The transmitted data bits from COM port of the computer are captured by Logical analyzer is as shows in Figure 1.8. FPGA results for decoding the UART data is shown in Figure 1.9.

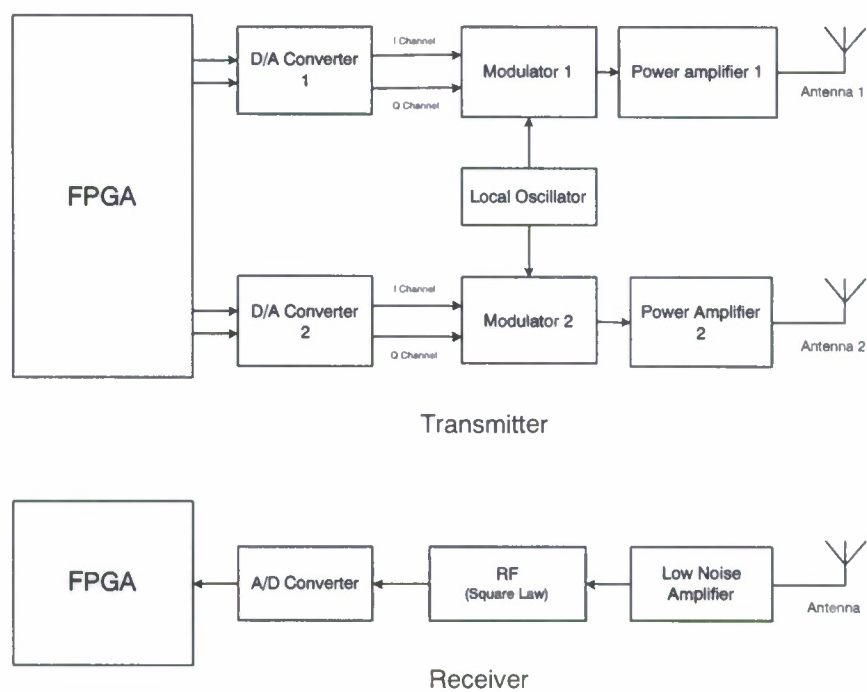


Figure 1.1: MISO UWB testbed architecture

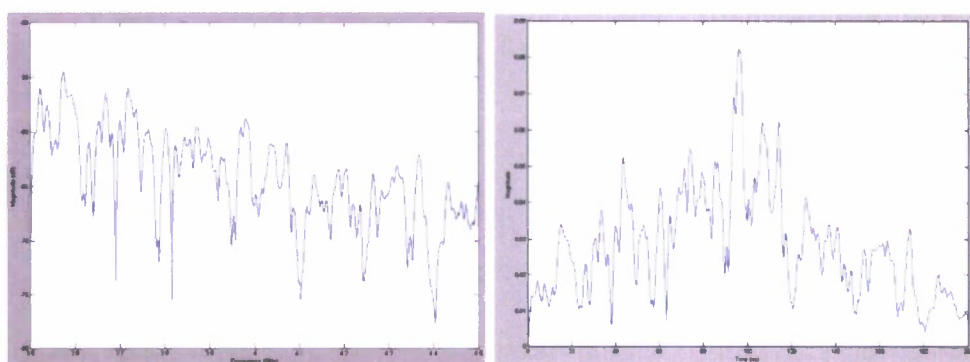


Figure 1.2: Channel 1 transfer function and corresponding baseband CIR

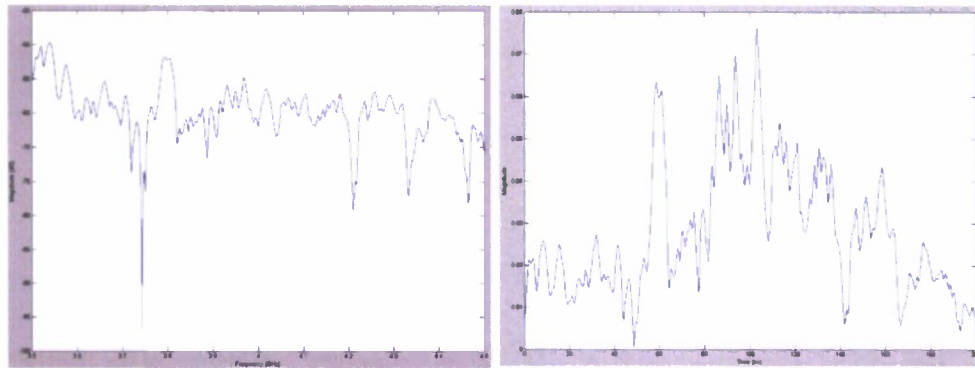


Figure 1.3: Channel 2 transfer function and corresponding baseband CIR



(a) SISO

(b) SISO

(c) MISO

Figure 1.4: The received waveforms after the RF board using time reversal waveform. (a) Only antenna 1 is transmitting. (b) Only antenna 2 is transmitting. (c) Antenna 1 and antenna 2 are both transmitting.

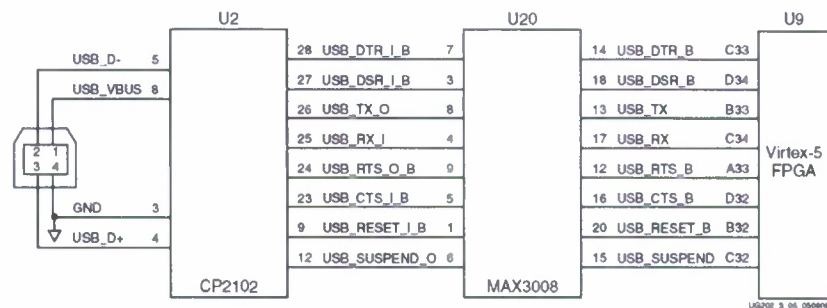


Figure 1.5: Diagram of the UART module on ML550 FPGA platform.



Figure 1.6: Frame structure of UART transmitting.

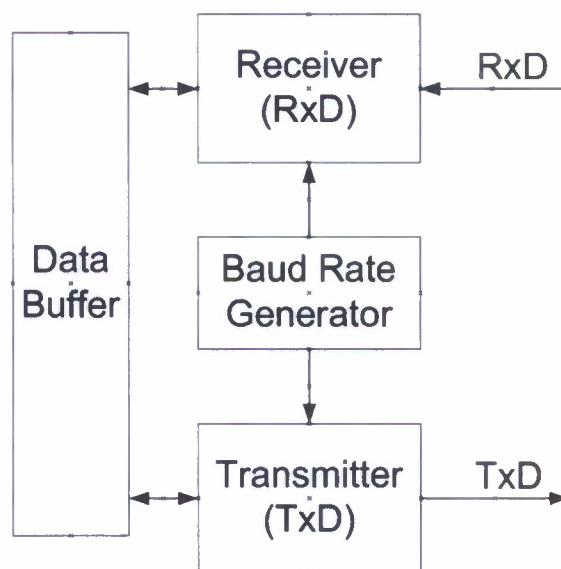


Figure 1.7: Simple diagram of the UART design.

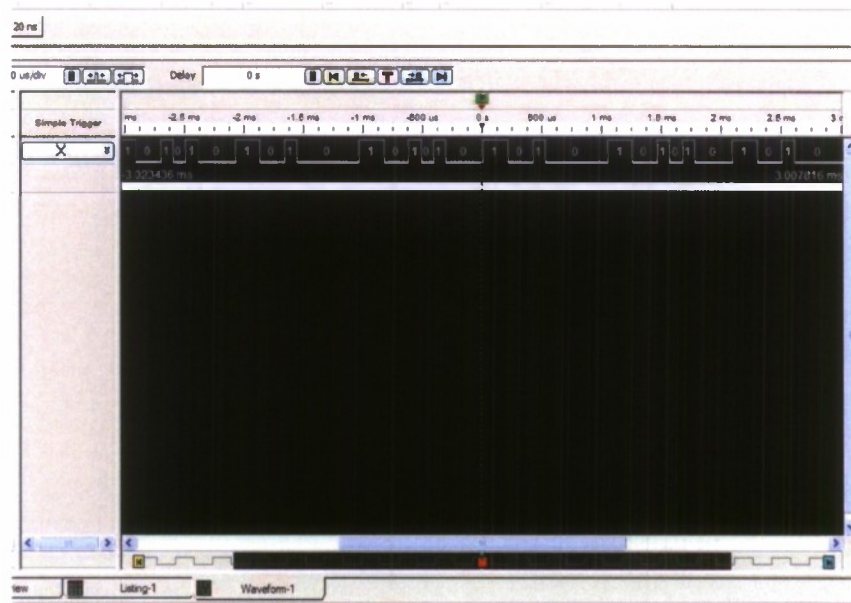


Figure 1.8: Captured UART signal by Logical Analyzer.

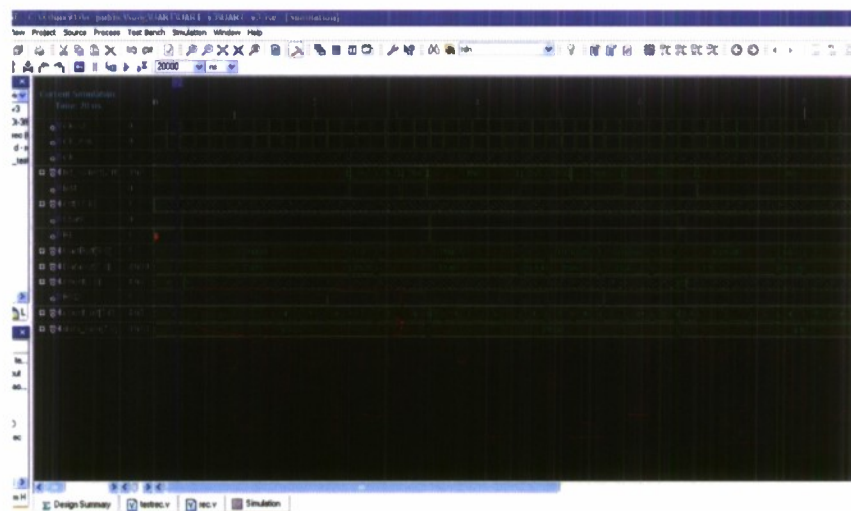


Figure 1.9: FPGA simulation results for decoding UART signal.

## **Chapter 2**

# **Wideband Multichannel Coherent Receiver Design**

### **2.1 Background**

The multichannel receiver is a building core for any MIMO system in either communication or radar. Especially from military perspective, there has been a critical and constant need for enhanced multichannel receivers for array and radar applications. More channels and bandwidth are required, while less power consumption, lower cost, and smaller sizes are expected. There is also a trend that the receivers are more and more digital, thanks to the advance in semiconductor technologies. Having seen so much progress in hardware, especially, dramatic increase of sampling rate in digital processing, newer type of receivers taking advantages of all possible new concepts and most advanced components/devices are expected. A variety of available technologies have to be considered and compromising has to be made among a large number of factors.

### **2.2 Overall Architecture**

Illustrated in Fig.1 is a high level receiver architecture containing three functional blocks: analog frontend (tuner), digitizer and digital backend. In choosing the sampling rate and determining digital computational load, we will attempt to be a little aggressive, expecting that digital processing power will increase while the cost will drop continuously. There are a number of options in selecting a digital processing platform. We prefer to use an array of high performance FPGAs such as Xilinx Virtex-5 or Virtex-6 series. This type of digital signal processing platform is particularly attracting for advanced digital receiver prototyping.

### **2.3 Analog Frontend (Tuner)**

In general there are two popular options for radio frontend architecture: heterodyne (or superheterodyne) and zero-IF (or direct-conversion, homodyne) architectures. The heterodyne architecture has better performance if compared

with the other, and therefore it has been the most popular receiver architecture since it was invented by Edwin H. Armstrong in 1918. On the other hand, although the concept of zero-IF reception was first proposed by F.M. Colebrook as early as in 1924 (6 years before the heterodyne receiver was invented), it was not until 1947 that it was put into practice, the first application being measurements in telephony. Since 90's, zero-IF architecture has been especially promoted in software defined radio (SDR) community. Compared with the traditional receiver architecture, its main advantages are the following:

- (1) The problem of image rejection is overcome, so that the receiver presclection portion is simplified and frequency planning is unnecessary.
- (3) The fact that most signal processing is done at low frequencies implies using LPFs as channel-select filters.
- (4) Amplification is mainly at the baseband stage, hence power is saved. In general, a zero-IF receiver contains less hardware and has very high level of integration.

While being attractive, the zero-IF receiver architecture has many drawbacks: DC offset, I/Q imbalance (or mismatching) with analog quadrature downconverter, even-order distortion, self-mixing,  $1/f$  (or clicker) noise, and local oscillator (LO) leakage. In order to combine the advantages of both the heterodyne and zero-IF architectures, a low-IF receiver architecture was proposed in later 90's. This architecture indeed keeps a high level of integration and eliminates most of the drawbacks associated with the zero-IF receivers, but it introduces image rejection requirement. When the RF frequencies are lower than 2 GHz (HF, VHF, UHF and L bands), the rather low IF frequency image rejection is difficult to implement and image rejection mixer techniques are required instead of an image rejection filter. In practical image rejection mixers, the amplitude and phase mismatches between I and Q channels are ultimate limitation of the image rejection ratio [3]. In addition, designing and implementing ultra wideband image rejection mixers is extremely difficult.

Although the low-IF structure has many advantages, it may not be feasible for UWB applications, due to the limitation of the digitizer's sampling rate. The zero-IF structure will be the first choice at present. In the future, low-IF can be considered if the digitizer's sampling rate significantly increases or the signal bandwidth is much less than 500 MHz.

## 2.4 Automatic Gain Control (AGC)

We propose to achieve the dynamic range through both RF and IF stages. Although the 52-dB dynamic range can be provided solely by the IF stage, variable amplification at the both stages has a few advantages: the overall dynamic range increases, and RF signal reduction can ease EMC issue and prevent the system from self-oscillating. There are not many off-the-shelf products of variable-gain amplifiers (VGAs) with GHz bandwidth. One RF VGA option is to combine an X-band amplifier with a wideband digital attenuator. If selecting Analog Devices ADL5330 to build IF stage, the IF VGA itself can provide a 60-dB dynamic range. This double loop AGC requires more peripheral control circuits than single-loop AGC, but it is not necessary to have dedicated control circuits for each

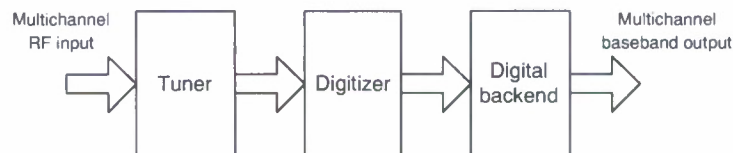


Figure 2.1: High level multichannel receiver architecture.

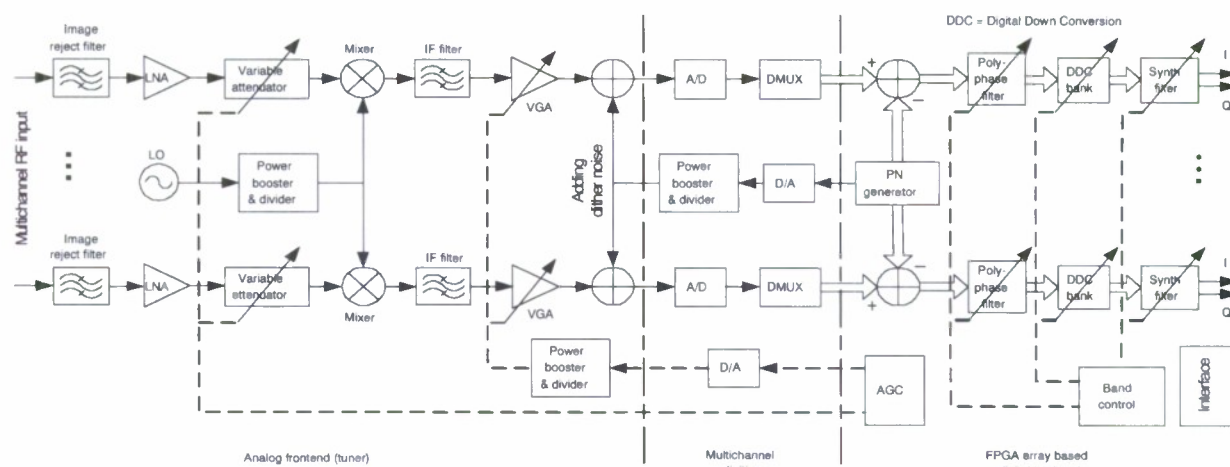


Figure 2.2: Proposed multichannel receiver architecture that can support both zero-IF and low-IF configurations.

channel. If all channels share a single double-loop AGC controller, the complexity contributed by the AGC part is very limited. The ADL5330 needs an analog signal to control the gain, and the control circuit can be implemented using a low-sampling D/A followed by a power booster and divider unit.

## 2.5 Digitizer Architecture

## 2.6 Sundance 4 channels digitizer system with FPGA processing

In last quarterly report, the digitizer selection has been briefly introduced. Finally, we chose the product SMT702 from Sundance, Inc to build the UWB multi-channels system.

The SMT702 is a PXI Express Peripheral Module (3U), which integrates two 3 Gsps 8-bit ADCs, a clock circuitry, 2 banks of 1GByte DDR2 Memory each and a Xilinx Virtex5 LX110T-3 FPGA, under the 3U format. The good news for this product is it can be standalone and with a number of general I/Os. Figure 2.3 shows the picture and diagram of SMT702.

Figure 2.4 shows the 4-channels system architecture consists of 5 SMT702 boards, each channel with both I phase and Q phase channel, each channel capable of handling 3Gsps sampling. In this architecture, the Sundance SHB cables will be used to connect all the boards.

The SMT702 is a PXI Express (opt. Hybrid) Peripheral Module (3U), which integrates two fast 8-bit ADCs, a clock circuitry, 2 banks of DDR2 Memory and a Virtex5 Xilinx FPGA, under the 3U format.

The PXIe specification integrates PCI Express signaling into the PXI standard for more backplane bandwidth. It also enhances PXI timing and synchronization features by incorporating a 100MHz differential reference clock and triggers. The SMT702 can also integrate the standard 32-bit PXI signaling as an option.

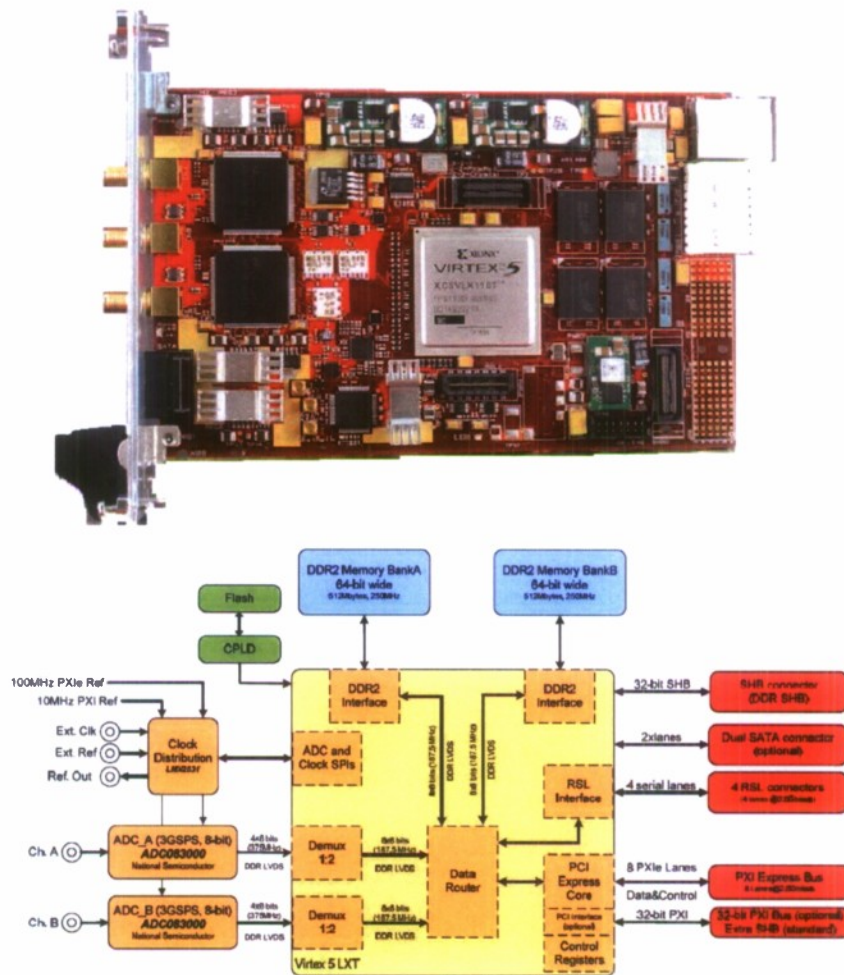


Figure 2.3: SMT702 board picture and functional diagram.

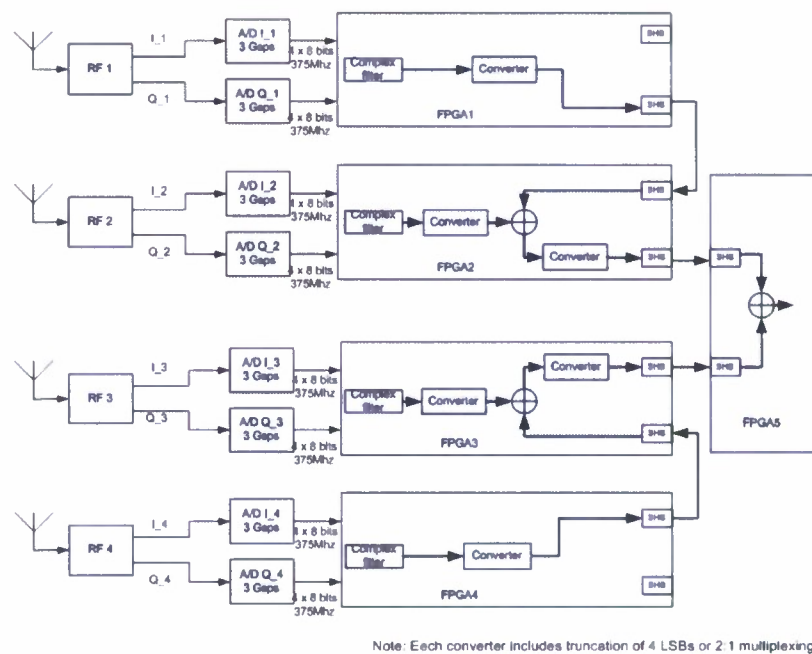


Figure 2.4: Wideband beamforming architecture with 5 SMT702 high speed digitizers.

Both ADC chips are identical and can produce 3 Giga-samples per second each, with an 8-bit resolution. The manufacturer is National Semiconductor and the part number is ADC083000. Analog-to-Digital converters are clocked by circuitry based on a PLL coupled with a VCO in order to generate a low-jitter signal. The full bandwidth is 3GHz. Each ADC integrates settings such as offset and scale factor, which makes the pair of ADC suitable to be combined together in order to make a 6GSPS single Analog to Digital converter. This will be subject to a specific application note.

An on-board PLL+VCO chip ensure a stable fixed sampling frequency (maximum rate), in order for the board to be used as a digitizer without the need of external clock signal. The PLL will be able to lock its internal VCO either on the 100MHz PXI express reference, on the 10MHz PXI reference or on an external reference signal. The sampling clock for the converters can be either coming from the PLL+VCO chip (fixed frequency of 1.5ghz) or from an external source. The chip used is a National Semiconductor part: LMX2531LQ1500. The reference clock selected is also output on a connector in order to pass it to an other module.

The Virtex5 FPGA is responsible for controlling all interfaces, including PXI (32-bit) and PXIe (up to 8 lanes not all PXI Express controller support 8 lane), as well as routing samples. The FPGA fitted on the SMT702 is part of the Virtex-5 family from Xilinx, XC5VLX110T-3 (fastest speed grade available).

Two DDR2 memory banks are accessible by the FPGA in order to store data on the fly. An SHB connector is available in order to transfer data/samples to an other Sundance module (SMT712 for instance). All analog connectors on the front panel are SMA.

For software development, the SMT7026 is an efficient, ready to use, host side interface for the SMT702. It allows us to control the SMT702 from the host as well as to exchange data between the host. It can configure the FPGA from the Host, transfer data from the SMT702 to the Host and even provide a C++ type interface to the FPGA module. A screen shot of the SMT7026 is shown as Figure 2.5.

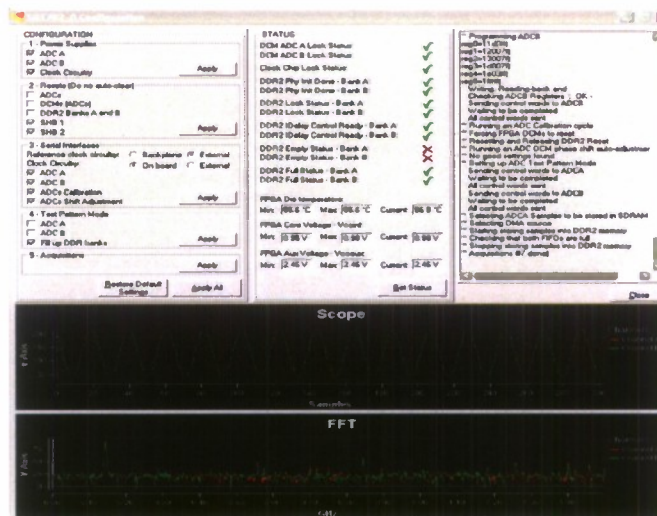


Figure 2.5: A screen capture of SMT7026 for SMT702 digitizer when sampling.

## Chapter 3

# Theoretical Work

### 3.1 Wideband Waveform Optimization for Multiple Input Single Output Cognitive Radio with Practical Consideration

#### 3.1.1 Introduction

Waveform design or optimization is a key research issue in the current wireless communication system, the radar system and the sensing or image system. Waveform should be designed according to the different requirements and objectives of system performance. For example, the waveform should be designed to carry more information to the receiver in terms of capacity. If the energy detector is employed at the receiver, the waveform should be optimized such that the energy of the signal in the integration window at the receiver should be maximized [4] [5] [6] [7]. For navigation and geolocation, the ultra short waveform should be used to increase the resolution. For multi-target identification, the waveform should be designed so that the radar returns can bring more information back. In clutter dominant environment, maximizing the target energy and minimizing the clutter energy should be considered. In electronic warfare, anti-jamming is the important task for the outcome of the warfare. Though currently anti-jamming is performed at the receiver, if the transmitter knows some kind of information about the jamming at the receiver, for example, the second order statistics about jamming, the transmitter can elaborately design the waveform and help receiver to cancel the jamming signal or save the energy.

In the context of cognitive radio, waveform design or optimization gives us more flexibilities to design radio, which can coexist with other cognitive radios and primary radios. From cognitive radio's point of view, spectral mask constraint at the transmitter and the interference cancellation at the receiver should be seriously considered for waveform design or optimization, in addition to the traditional communication objectives and constraints. Spectral mask constraint is imposed on the transmitted waveform such that cognitive radio has no interference to primary radio. At the same time the arbitrary notch filter is implemented at the receiver to cancel the interference from primary radio to cognitive radio.

Multiple Input Single Output (MISO) system considered in this section is one kind of multi-antenna system in which there are multiple antennas at the transmitter and one antenna at the receiver. MISO system can explore the spatial diversity and execute the beamforming to focus energy on the desired direction or point and avoid interference to other radio systems. It is well known that waveform and spatially diverse capabilities are made possible today due

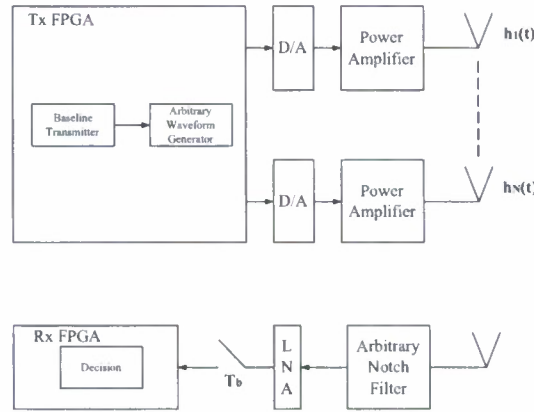


Figure 3.1: System architecture.

to the advent of lightweight digital programming waveform generator [8] or arbitrary waveform generator.

This section deals with wideband waveform optimization for MISO cognitive radio. Cauchy–Schwarz inequality-based iterative method and Semidefinite Programming (SDP)-based iterative method are exploited to take care of wideband waveform design. Both of them can give the optimal solutions [7]. Different designed waveforms are to be applied to different antennas. But these waveforms are optimized jointly in order to match the different spatial channels based on the objective of the system performance. SDP-based signal processing is becoming more and more popular recently. It can be applied to control theory, statistics, circuit design, graph theory and so on. The reasons for this is (1) more and more practical problems can be formulated as SDP; (2) most interior-point methods for linear programming have been generalized to SDP [9]; (3) nowadays the computational capability is increased greatly and SDP can be solved in real-time. Meanwhile, reduction in transmitted peak power and quantization is still very desirable, being concerned about the implementation complexity and power consumption. Thus, Peak-to-Average Power Ratio (PAPR) and binary waveform design are taken into account as the practical considerations in the context of MISO cognitive radio.

### 3.1.2 Wideband Waveform Optimization Using Cauchy–Schwarz Inequality-based Iterative Method

The system architecture considered in this section is shown in Figure 3.1. We limit our discussion to a single pair of cognitive radios scenario. There are  $N$  antennas at the transmitter and one antenna at the receiver. On-off keying (OOK) modulation is used for transmission. Thus the transmitted signal at the transmitter antenna  $n$  is,

$$s_n(t) = \sum_{j=-\infty}^{\infty} d_j p_n(t - jT_b) \quad (3.1)$$

where  $T_b$  is the bit duration,  $p_n(t)$  is the transmitted bit waveform defined over  $[0, T_p]$  at the transmitter antenna  $n$  and  $d_j \in \{0, 1\}$  is  $j$ -th transmitted bit. Without loss of generality, the minimal propagation delay is assumed to be zero. The energy of transmitted waveforms is  $E_p$ ,

$$\sum_{n=1}^N \int_0^{T_p} p_n^2(t) df = E_p \quad (3.2)$$

The received noise-polluted signal at the output of low noise amplifier (LNA) is,

$$\begin{aligned} r(t) &= \sum_{n=1}^N h_n(t) \otimes s_n(t) + n(t) \\ &= \sum_{j=-\infty}^{\infty} d_j \sum_{n=1}^N x_n(t - jT_b) + n(t) \end{aligned} \quad (3.3)$$

where  $h_n(t)$ ,  $t \in [0, T_h]$  is the multipath impulse response that takes into account the effect of channel impulse response, the RF front-ends in the transceivers such as power amplifier, LNA and arbitrary notch filter as well as antennas between the transmitter antenna  $n$  and the receiver antenna.  $h_n(t)$  is available at the transmitter [10] [11].  $\int_0^{T_h} h_n^2(t) dt = E_{nh}$ . " $\otimes$ " denotes convolution operation.  $n(t)$  is AWGN.  $x_n(t)$  is the received noiseless bit-"1" waveform defined as

$$x_n(t) = h_n(t) \otimes p_n(t) \quad (3.4)$$

We further assume that  $T_b \geq T_h + T_p \stackrel{\text{def}}{=} T_x$ , i.e. no existence of ISI.

If the waveforms at different transmitter antennas are assumed to be synchronized, the  $k$ -th decision statistic is,

$$\begin{aligned} r(kT_b + t_0) &= \sum_{j=-\infty}^{\infty} d_j \sum_{n=1}^N x_n(kT_b + t_0 - jT_b) + n(t) \\ &= d_k \sum_{n=1}^N x_n(t_0) + n(t) \end{aligned} \quad (3.5)$$

In order to maximize the system performance,  $\sum_{n=1}^N x_n(t_0)$  should be maximized. Thus the optimization problem can be formulated as follows to get the optimal waveforms  $p_n(t)$ ,

$$\begin{aligned} &\text{maximize } \sum_{n=1}^N x_n(t_0) \\ &\text{subject to} \\ &\sum_{n=1}^N \int_0^{T_p} p_n^2(t) dt \leq E_p \\ &0 \leq t_0 \leq T_b \end{aligned} \quad (3.6)$$

An iterative method is proposed here to give the optimal solution to the optimization problem (3.6). This method is a computationally efficient algorithm. For simplicity in the following presentation,  $t_0$  is assumed to be zero, which will not degrade the optimum of the solution if such solution exists.

$$x(t) = \sum_{n=1}^N x_n(t) \quad (3.7)$$

From inverse Fourier transform,

$$x_{nf}(f) = h_{nf}(f) p_{nf}(f) \quad (3.8)$$

and

$$x_f(f) = \sum_{n=1}^N h_{nf}(f) p_{nf}(f) \quad (3.9)$$

where  $x_{nf}(f)$ ,  $h_{nf}(f)$  and  $p_{nf}(f)$  are the frequency domain representations of  $x_n(t)$ ,  $h_n(t)$  and  $p_n(t)$  respectively.  $x_f(f)$  is frequency domain representation of  $x(t)$ . Thus,

$$x(0) = \sum_{n=1}^N x_n(0) \quad (3.10)$$

and,

$$x_n(0) = \int_{-\infty}^{\infty} x_{nf}(f) df \quad (3.11)$$

If there is no spectral mask constraint, then according to the Cauchy–Schwarz inequality,

$$\begin{aligned} x(0) &= \sum_{n=1}^N \int_{-\infty}^{\infty} h_{nf}(f) p_{nf}(f) df \\ &\leq \sum_{n=1}^N \sqrt{\int_{-\infty}^{\infty} |h_{nf}(f)|^2 df} \sqrt{\int_{-\infty}^{\infty} |p_{nf}(f)|^2 df} \\ &\leq \sqrt{\sum_{n=1}^N \int_{-\infty}^{\infty} |h_{nf}(f)|^2 df} \sqrt{\sum_{n=1}^N \int_{-\infty}^{\infty} |p_{nf}(f)|^2 df} \\ &= \sqrt{E_p \sum_{n=1}^N E_{nh}} \end{aligned} \quad (3.12)$$

when  $p_{nf}(f) = \alpha h_{nf}(f)$  for all  $f$  and  $n$ , two equalities are obtained.

$$\alpha = \sqrt{\frac{E_p}{\sum_{n=1}^N \int_{-\infty}^{\infty} |h_{nf}(f)|^2 df}} \quad (3.13)$$

In this case,  $p_n(t) = \alpha h_n(-t)$ , which means the optimal waveform  $p_n(t)$  is the corresponding time reversed multipath impulse response  $h_n(t)$ .

If there is spectral mask constraint, then the following optimization problem will become more complicated,

$$\begin{aligned} &\text{maximize } x(0) \\ &\text{subject to} \\ &\sum_{n=1}^N \int_0^{T_p} p_n^2(t) dt \leq E_p \\ &|p_{nf}(f)|^2 \leq c_{nf}(f) \end{aligned} \quad (3.14)$$

where  $c_{nf}(f)$  represents the arbitrary spectral mask constraint at the transmitter antenna  $n$ .

Because  $p_{nf}(f)$  is the complex value, the phase and the modulus of  $p_{nf}(f)$  should be determined.

Meanwhile,

$$x(0) = \int_{-\infty}^{\infty} x_f(f) df \quad (3.15)$$

and,

$$x_f(f) = \sum_{n=1}^N |h_{nf}(f)| |p_{nf}(f)| e^{j2\pi(\arg(h_{nf}(f)) + \arg(p_{nf}(f)))} \quad (3.16)$$

where the angular component of the complex value is  $\arg(\bullet)$ .

For the real value signal  $x(t)$ ,

$$x_f(f) = x_f^*(-f) \quad (3.17)$$

where “\*” denotes conjugate operation. Thus,

$$x_f(-f) = \sum_{n=1}^N |h_{nf}(f)| |p_{nf}(f)| e^{-j2\pi(\arg(h_{nf}(f)) + \arg(p_{nf}(f)))} \quad (3.18)$$

and  $x_f(f) + x_f(-f)$  is equal to

$$\sum_{n=1}^N |h_{nf}(f)| |p_{nf}(f)| \cos(2\pi(\arg(h_{nf}(f)) + \arg(p_{nf}(f)))) \quad (3.19)$$

If  $h_{nf}(f)$  and  $|p_{nf}(f)|$  are given for all  $f$  and  $n$ , maximization of  $x(0)$  is equivalent to,

$$\arg(h_{nf}(f)) + \arg(p_{nf}(f)) = 0 \quad (3.20)$$

which means the angular component of  $p_{nf}(f)$  is the negative angular component of  $h_{nf}(f)$ .

The optimization problem (3.14) can be simplified as,

$$\begin{aligned} & \text{maximize} \quad \sum_{n=1}^N \int_{-\infty}^{\infty} |h_{nf}(f)| |p_{nf}(f)| df \\ & \text{subject to} \\ & \quad \sum_{n=1}^N \int_{-\infty}^{\infty} |p_{nf}(f)|^2 df \leq E_p \\ & \quad |p_{nf}(f)|^2 \leq c_{nf}(f) \end{aligned} \quad (3.21)$$

Because,

$$|h_{nf}(f)| = |h_{nf}(-f)| \quad (3.22)$$

$$|p_{nf}(f)| = |p_{nf}(-f)| \quad (3.23)$$

$$|c_{nf}(f)| = |c_{nf}(-f)| \quad (3.24)$$

for all  $f$  and  $n$ . Thus uniformly discrete frequency points  $f_0, \dots, f_M$  are considered in the optimization problem (3.21). Meanwhile,  $f_0$  corresponds to the DC component and  $f_1, \dots, f_M$  correspond to the positive frequency components.

Define column vectors  $\mathbf{h}_f, \mathbf{h}_{1f}, \dots, \mathbf{h}_{Nf}$ ,

$$\mathbf{h}_f = [\mathbf{h}_{1f}^T \mathbf{h}_{2f}^T \dots \mathbf{h}_{Nf}^T]^T \quad (3.25)$$

$$(\mathbf{h}_{nf})_i = \begin{cases} |h_{nf}(f_{i-1})|, i = 1 \\ \sqrt{2} |h_{nf}(f_{i-1})|, i = 2, \dots, M + 1 \end{cases} \quad (3.26)$$

where “ $T$ ” denotes transpose operation.

Define column vectors  $\mathbf{p}_f, \mathbf{p}_{1f}, \dots, \mathbf{p}_{Nf}$ ,

$$\mathbf{p}_f = [\mathbf{p}_{1f}^T \mathbf{p}_{2f}^T \dots \mathbf{p}_{Nf}^T]^T \quad (3.27)$$

$$(\mathbf{p}_{nf})_i = \begin{cases} |p_{nf}(f_{i-1})|, i = 1 \\ \sqrt{2} |p_{nf}(f_{i-1})|, i = 2, \dots, M + 1 \end{cases} \quad (3.28)$$

Define column vectors  $\mathbf{c}_f, \mathbf{c}_{1f}, \dots, \mathbf{c}_{Nf}$ ,

$$\mathbf{c}_f = [\mathbf{c}_{1f}^T \mathbf{c}_{2f}^T \dots \mathbf{c}_{Nf}^T]^T \quad (3.29)$$

$$(\mathbf{c}_{nf})_i = \begin{cases} \sqrt{|c_{nf}(f_{i-1})|}, i = 1 \\ \sqrt{2} |c_{nf}(f_{i-1})|, i = 2, \dots, M + 1 \end{cases} \quad (3.30)$$

Thus, the discrete version of the optimization problem (3.21) is shown below,

$$\begin{aligned} & \text{maximize } \mathbf{h}_f^T \mathbf{p}_f \\ & \text{subject to} \\ & \|\mathbf{p}_f\|_2^2 \leq E_p \\ & 0 \leq \mathbf{p}_f \leq \mathbf{c}_f \end{aligned} \quad (3.31)$$

An iterative method (Algorithm I) is shown as follows to give the optimal solution  $\mathbf{p}_f^*$  to the optimization problem (3.31), which was proposed in [7] and is extended to waveform design in the context of MISO cognitive radio:

1. Initialization:  $P = E_p$  and  $\mathbf{p}_f^*$  is set to be all-0 column vector.
2. Solve the following optimization problem to get the optimal  $\mathbf{q}_f^*$  using Cauchy–Schwarz inequality.

$$\begin{aligned} & \text{maximize } \mathbf{h}_f^T \mathbf{q}_f \\ & \text{subject to} \\ & \|\mathbf{q}_f\|_2^2 \leq P \end{aligned} \quad (3.32)$$

3. Find  $i$ , such that  $(\mathbf{q}_f^*)_i$  is the maximal value in the set  $\left\{ (\mathbf{q}_f^*)_j \mid (\mathbf{q}_f^*)_j > (\mathbf{c}_f)_j \right\}$ . If  $\{i\} = \emptyset$ , then the method is terminated and  $\mathbf{p}_f^* := \mathbf{p}_f^* + \mathbf{q}_f^*$ . Otherwise go to step 4.

4. Set  $(\mathbf{p}_f^*)_i = (\mathbf{c}_f)_i$ .

5.  $P := P - (\mathbf{c}_f)_i^2$  and set  $(\mathbf{h}_f)_i$  to zero. If  $\|\mathbf{h}_f\|_2^2$  is equal to zero, then the method is terminated. Otherwise go to step 2.

When  $\mathbf{p}_f^*$  is obtained for the optimization problem (3.31), from Eq. (3.20), Eq. (3.27) and Eq. (3.28), the optimal  $p_{nf}(f)$  and the corresponding  $p_n(t)$  can be smoothly achieved.

### 3.1.3 Wideband Waveform Optimization Using SDP-based Iterative method

The  $p_n(t)$  and the  $h_n(t)$  are uniformly sampled at Nyquist rate. Assume the sampling period is  $T_s$ .  $T_p/T_s = N_p$  and  $N_p$  is assumed to be even,  $T_h/T_s = N_h$ .  $p_n(t)$  and  $h_n(t)$  are represented by  $p_{ni}, i = 0, 1, \dots, N_p$  and  $h_{ni}, i = 0, 1, \dots, N_h$  respectively.

Define,

$$\mathbf{p}_n = [p_{n0} \ p_{n1} \ \cdots \ p_{nN_p}]^T \quad (3.33)$$

and

$$\mathbf{h}_n = [h_{nN_h} \ h_{n(N_h-1)} \ \cdots \ h_{n0}]^T \quad (3.34)$$

If  $N_p = N_h$ , then  $\sum_{n=1}^N x_n(t_0)$  can be equivalent to  $\sum_{n=1}^N \mathbf{h}_n^T \mathbf{p}_n$ . Define,

$$\mathbf{P} = [\mathbf{p}_1^T \ \mathbf{p}_2^T \ \cdots \ \mathbf{p}_N^T]^T \quad (3.35)$$

and

$$\mathbf{h} = [\mathbf{h}_1^T \ \mathbf{h}_2^T \ \cdots \ \mathbf{h}_N^T]^T \quad (3.36)$$

Thus,

$$\sum_{n=1}^N \mathbf{h}_n^T \mathbf{p}_n = \mathbf{h}^T \mathbf{P} \quad (3.37)$$

Maximization of  $\mathbf{h}^T \mathbf{P}$  is the same as maximization of  $(\mathbf{h}^T \mathbf{P})^2$  as long as  $\mathbf{h}^T \mathbf{P}$  is equal to or greater than zero.

$$\begin{aligned} (\mathbf{h}^T \mathbf{P})^2 &= (\mathbf{h}^T \mathbf{P})^T (\mathbf{h}^T \mathbf{P}) \\ &= \mathbf{P}^T \mathbf{h} \mathbf{h}^T \mathbf{P} \\ &= \text{trace}(\mathbf{h} \mathbf{h}^T \mathbf{P} \mathbf{P}^T) \\ &= \text{trace}(\mathbf{H} \mathbf{P}) \end{aligned} \quad (3.38)$$

where  $\mathbf{H} = \mathbf{h} \mathbf{h}^T$  and  $\mathbf{P} = \mathbf{P} \mathbf{P}^T$ .  $\mathbf{P}$  should be rank-1 positive semidefinite matrix. However, rank constraint is non-convex constraint, which will be omitted in the following optimization problems. Thus the optimization objective in the optimization problem (3.14) can be reformulated as,

$$\text{maximize trace}(\mathbf{H} \mathbf{P}) \quad (3.39)$$

Meanwhile,

$$\begin{aligned} \|\mathbf{P}\|_2^2 &= \mathbf{P}^T \mathbf{P} \\ &= \text{trace}(\mathbf{P} \mathbf{P}^T) \\ &= \text{trace}(\mathbf{P}) \end{aligned} \quad (3.40)$$

Thus the energy constraint in the optimization problem (3.14) can be reformulated as,

$$\text{trace}(\mathbf{P}) \leq E_p \quad (3.41)$$

For cognitive radio, there is a spectral mask constraint for the transmitted waveform. Based on the previous discussion,  $\mathbf{p}_n$  is assumed to be the transmitted waveform, and  $\mathbf{F}$  is the discrete-time Fourier transform operator, thus the frequency domain representation of  $\mathbf{p}_n$  is,

$$\mathbf{p}_{fn} = \mathbf{F}\mathbf{p}_n \quad (3.42)$$

where  $\mathbf{p}_{fn}$  is a complex value vector. If the  $i$ -th row of  $\mathbf{F}$  is  $\mathbf{f}_i$ , then each complex value in  $\mathbf{p}_{fn}$  can be represented by,

$$(\mathbf{p}_{fn})_{i,1} = \mathbf{f}_i \mathbf{p}_n, i = 1, 2, \dots, \frac{N_p}{2} + 1 \quad (3.43)$$

Define,

$$\mathbf{F}_i = \mathbf{f}_i^H \mathbf{f}_i, i = 1, 2, \dots, \frac{N_p}{2} + 1 \quad (3.44)$$

Given the spectral mask constraint in terms of power spectral density  $\mathbf{c}_n = [c_{n1} c_{n2} \dots c_{n \frac{N_p}{2} + 1}]^T$ , so

$$\begin{aligned} |(\mathbf{p}_{fn})_{i,1}|^2 &= |\mathbf{f}_i \mathbf{p}_n|^2 \\ &= \mathbf{p}_n^T \mathbf{f}_i^H \mathbf{f}_i \mathbf{p}_n \\ &= \mathbf{p}_n^T \mathbf{F}_i \mathbf{p}_n \\ &\leq c_{ni}, i = 1, 2, \dots, \frac{N_p}{2} + 1 \end{aligned} \quad (3.45)$$

where  $|\bullet|$  is the modulus of the complex value.

Define selection matrix  $\mathbf{S}_n \in R^{(N_p+1) \times (N_p+1)N}$ ,

$$(\mathbf{S}_n)_{i,j} = \begin{cases} 1, & j = i + (N_p + 1)(n - 1) \\ 0, & \text{else} \end{cases} \quad (3.46)$$

So,

$$\mathbf{p}_n = \mathbf{S}_n \mathbf{p} \quad (3.47)$$

and

$$\begin{aligned} |(\mathbf{p}_{fn})_{i,1}|^2 &= \mathbf{p}_n^T \mathbf{F}_i \mathbf{p}_n \\ &= \mathbf{p}^T \mathbf{S}_n^T \mathbf{F}_i \mathbf{S}_n \mathbf{p} \\ &= \text{trace}(\mathbf{S}_n^T \mathbf{F}_i \mathbf{S}_n \mathbf{p} \mathbf{p}^T) \\ &= \text{trace}(\mathbf{S}_n^T \mathbf{F}_i \mathbf{S}_n \mathbf{P}) \end{aligned} \quad (3.48)$$

The optimization problem (3.14) can be reformulated as SDP based on (3.39), (3.41), (3.45) and (3.48),

$$\begin{aligned} &\text{maximize trace}(\mathbf{H}\mathbf{P}) \\ &\text{subject to} \\ &\text{trace}(\mathbf{P}) \leq E_p \\ &\text{trace}(\mathbf{S}_n^T \mathbf{F}_i \mathbf{S}_n \mathbf{P}) \leq c_{ni} \\ &i = 1, 2, \dots, \frac{N_p+1}{2} \\ &n = 1, 2, \dots, N \end{aligned} \quad (3.49)$$

If the optimal solution  $\mathbf{P}^*$  to the optimization problem (3.49) is the rank-1 matrix, then the optimal waveforms can be obtained from the dominant eigen-vector of  $\mathbf{P}^*$ . Otherwise,  $E_p$  in the optimization problem (3.49) should be decreased to get the rank-1 optimal solution  $\mathbf{P}^*$  to satisfy all the other constraints.

An SDP-based iterative method (Algorithm II) is proposed to get the rank-1 optimal solution  $\mathbf{P}^*$ :

1. Initialization of  $E_p$ .
2. Solve the optimization problem (3.49) and get the optimal solution  $\mathbf{P}^*$ .
3. If the ratio of dominant eigen-value of  $\mathbf{P}^*$  to trace ( $\mathbf{P}^*$ ) is less than 0.99, then set  $E_p$  to be trace ( $\mathbf{P}^*$ ) and go to step 2. Otherwise, the method is terminated.

The optimal waveforms can be obtained from the dominant eigen-vector of  $\mathbf{P}^*$ , the dominant eigen-value of  $\mathbf{P}^*$  and Eq. (3.35).

### 3.1.4 Waveform Design with Practical Considerations

#### Peak-to-Average Power Ratio

PAPR is one of major concerns in waveform design. Because of nonlinearity caused by nonlinear devices such as Digital-to-Analog Converter (DAC) and Power Amplifier (PA), maximal transmitted power has to be backed up, resulting in inefficient utilization. PAPR in OFDM has been well studied. In this section, PAPR is handled under a unified optimization framework. It is defined as,

$$\text{PAPR} = \frac{\|\mathbf{p}_n\|_\infty^2}{\|\mathbf{p}_n\|_2^2 / (N_p + 1)} \quad (3.50)$$

where

$$\|\mathbf{p}_n\|_\infty = \max(|p_{n0}|, |p_{n1}|, \dots, |p_{nN_p}|) \quad (3.51)$$

If the denominator of Eq. (3.50) is omitted, reducing PAPR is equivalent to setting the upper bound for  $\|\mathbf{p}_n\|_\infty$ . The bound constraint  $\|\mathbf{p}_n\|_\infty \leq b_n$  can also be written as,

$$-b_n \leq p_{ni} \leq b_n, i = 0, 1, \dots, N_p \quad (3.52)$$

which can be further simplified as,

$$p_{ni}^2 \leq (b_n)^2, i = 0, 1, \dots, N_p \quad (3.53)$$

Define selection vector  $\mathbf{s}_{ni} \in R^{1 \times (N_p + 1)N}$ ,

$$(\mathbf{s}_{ni})_{1,j} = \begin{cases} 1, & j = i + (N_p + 1)(n - 1) \\ 0, & \text{else} \end{cases} \quad (3.54)$$

So,

$$\mathbf{p}_{ni} = \mathbf{s}_{ni} \mathbf{P} \quad (3.55)$$

and

$$\begin{aligned}
 p_{ni}^2 &= \mathbf{P}_{ni}^2 \\
 &= (\mathbf{s}_{ni}\mathbf{P})^2 \\
 &= (\mathbf{s}_{ni}\mathbf{P})^T (\mathbf{s}_{ni}\mathbf{P}) \\
 &= \mathbf{P}^T \mathbf{s}_{ni}^T \mathbf{s}_{ni} \mathbf{P} \\
 &= \text{trace}(\mathbf{s}_{ni}^T \mathbf{s}_{ni} \mathbf{P} \mathbf{P}^T) \\
 &= \text{trace}(\mathbf{s}_{ni}^T \mathbf{s}_{ni} \mathbf{P})
 \end{aligned} \tag{3.56}$$

The optimization problem (3.14) or the optimization problem (3.49) together with PAPR consideration can be presented as SDP,

$$\begin{aligned}
 &\text{maximize trace}(\mathbf{H}\mathbf{P}) \\
 &\text{subject to} \\
 &\text{trace}(\mathbf{P}) \leq E_p \\
 &\text{trace}(\mathbf{S}_n^T \mathbf{F}_i \mathbf{S}_n \mathbf{P}) \leq c_{ni} \\
 &\text{trace}(\mathbf{s}_{ni}^T \mathbf{s}_{ni} \mathbf{P}) \leq b_n \\
 &i = 1, 2, \dots, \frac{N_P+1}{2} \\
 &n = 1, 2, \dots, N
 \end{aligned} \tag{3.57}$$

Similarly, if the optimal solution  $\mathbf{P}^*$  to the optimization problem (3.57) is the rank-1 matrix, then the optimal waveforms can be obtained from the dominant eigen-vector of  $\mathbf{P}^*$ . Otherwise,  $E_p$  in the optimization problem (3.57) should be decreased to get the rank-1 optimal solution  $\mathbf{P}^*$  to satisfy all the other constraints.

An SDP-based iterative method (Algorithm III) is proposed to get the rank-1 optimal solution  $\mathbf{P}^*$ :

1. Initialization of  $E_p$ .
2. Solve the optimization problem (3.57) and get the optimal solution  $\mathbf{P}^*$ .
3. If the ratio of dominant eigen-value of  $\mathbf{P}^*$  to trace( $\mathbf{P}^*$ ) is less than 0.99, then set  $E_p$  to be trace( $\mathbf{P}^*$ ) and go to step 2. Otherwise, the method is terminated.

The optimal waveforms can be obtained from the dominant eigen-vector of  $\mathbf{P}^*$ , the dominant eigen-value of  $\mathbf{P}^*$  and Eq. (3.35).

### Binary Waveform

If the transmitted waveform is constrained to the binary waveform because of the hardware limitation or implementation simplicity, or equivalently if  $p_{ni}^2 = \frac{E_p}{(N_P+1)N}$ , then The optimization problem (3.14) or the optimization

problem (3.49) together with binary waveform design can be formulated as SDP,

$$\begin{aligned}
 & \text{maximize trace}(\mathbf{HP}) \\
 & \text{subject to} \\
 & \text{trace}(\mathbf{P}) = E_p \\
 & \text{trace}(\mathbf{S}_n^T \mathbf{F}_i \mathbf{S}_n \mathbf{P}) \leq c_{ni} \\
 & \text{trace}(\mathbf{s}_{ni}^T \mathbf{s}_{ni} \mathbf{P}) = \frac{E_p}{(N_p+1)N} \\
 & i = 1, 2, \dots, \frac{N_p+1}{2} \\
 & n = 1, 2, \dots, N
 \end{aligned} \tag{3.58}$$

However, the constraints  $\text{trace}(\mathbf{P}) = E_p$  and  $\text{trace}(\mathbf{s}_{ni}^T \mathbf{s}_{ni} \mathbf{P}) = \frac{E_p}{(N_p+1)N}$  usually bring non-rank-1 optimal solution  $\mathbf{P}^*$  or invalid solution, i.e. no feasible region for the optimization problem because of the constraints, to the optimization problem (3.58). Thus the equality constraints are relaxed to the inequality constraints and the optimization problem (3.58) is relaxed to,

$$\begin{aligned}
 & \text{maximize trace}(\mathbf{HP}) \\
 & \text{subject to} \\
 & \text{trace}(\mathbf{P}) \leq E_p \\
 & \text{trace}(\mathbf{S}_n^T \mathbf{F}_i \mathbf{S}_n \mathbf{P}) \leq c_{ni} \\
 & \text{trace}(\mathbf{s}_{ni}^T \mathbf{s}_{ni} \mathbf{P}) \leq \frac{E_p}{(N_p+1)N} \\
 & i = 1, 2, \dots, \frac{N_p+1}{2} \\
 & n = 1, 2, \dots, N
 \end{aligned} \tag{3.59}$$

However, such relaxation forces us to verify the feasibility of the optimal solution  $\mathbf{P}^*$  to the optimization problem (3.59). If the dominant eigen-value of  $\mathbf{P}^*$  is the same as  $E_p$ , which means  $\text{trace}(\mathbf{s}_{ni}^T \mathbf{s}_{ni} \mathbf{P})$  is equal to  $\frac{E_p}{(N_p+1)N}$  for all  $i$  and  $n$ , then the optimal solution  $\mathbf{P}^*$  is feasible and the optimal binary waveforms can be obtained from the dominant eigen-vector of  $\mathbf{P}^*$  and the dominant eigen-value of  $\mathbf{P}^*$ . Otherwise,  $E_p$  in the optimization problem (3.59) should be decreased.

An SDP-based iterative method (Algorithm IV) is proposed to get the rank-1 optimal solution  $\mathbf{P}^*$ :

1. Initialization of  $E_p$ .
2. Solve the optimization problem (3.59) and get the optimal solution  $\mathbf{P}^*$ .
3. If the ratio of dominant eigen-value of  $\mathbf{P}^*$  to  $E_p$  is less than 0.9999, then set  $E_p$  to be  $\text{trace}(\mathbf{P}^*)$  and go to step 2. Otherwise, the method is terminated.

The optimal waveforms can be obtained from the dominant eigen-vector of  $\mathbf{P}^*$ , the dominant eigen-value of  $\mathbf{P}^*$  and Eq. (3.35).

### 3.1.5 Numerical Results

The following setting has been used in generating numerical results:  $T_s = 1ns$ ,  $T_h = 100ns$ ,  $T_p = 100ns$ ;  $E_p$  is set to be 1 as the initial value; the number of transmitter antennas  $N$  is equal to 2. Multipath impulse responses

represented in the frequency domain between transmitter antennas and receiver antenna are shown in Fig. 3.2. The nulling part from  $290\text{MHz}$  to  $390\text{MHz}$  in Fig. 3.2 emulates the effect of arbitrary notch filter at the receiver, which means there is interference from primary radio in this kind of notched frequency band. All the SDPs presented in this section are solved by the CVX tool [12] [13].

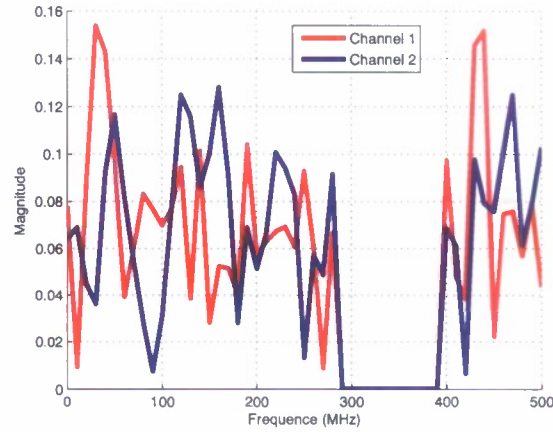


Figure 3.2: Multipath impulse responses represented in the frequency domain between transmitter antennas and receiver antenna.

Fig. 3.3 and Fig. 3.4 show designed optimal waveforms represented in frequency domain for two antennas respectively using Cauchy–Schwarz inequality-based iterative method (Algorithm I) and SDP-based iterative method (Algorithm II). The two methods give the same optimal solutions. Obtained from the designed optimal waveforms, there are no powers allocated to the notched frequency band for two transmitter antennas. The powers allocated to the notched frequency band can not bring any benefit to the performance. Meanwhile, all the spectral mask constraints are satisfied.

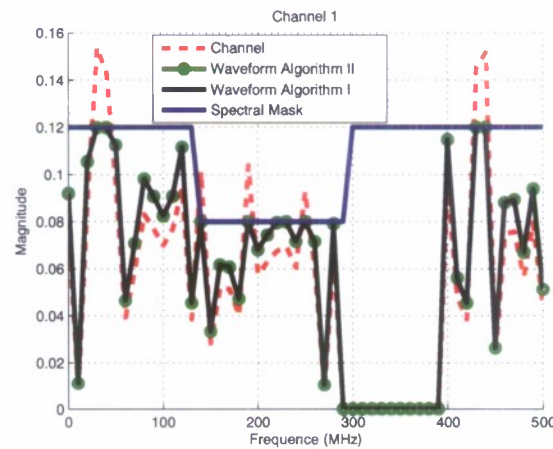


Figure 3.3: Designed waveform represented in frequency domain for channel 1.

Fig. 3.5 and Fig. 3.6 show designed optimal waveforms represented in frequency domain for two antennas respectively with PAPR consideration. Fig. 3.7 and Fig. 3.8 show designed optimal waveforms in correspondingly time

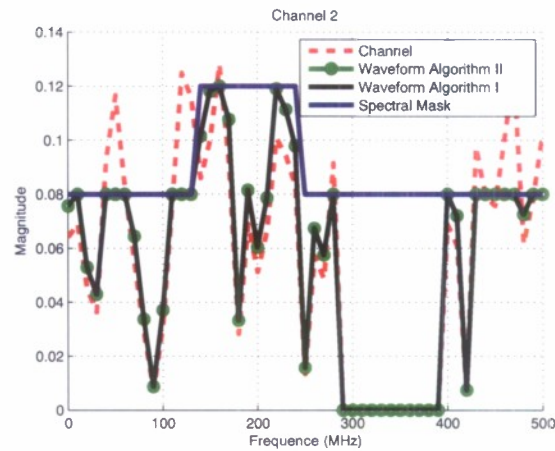


Figure 3.4: Designed waveform represented in frequency domain for channel 2.

domain for two antennas respectively. In this case,  $b_1$  is set to be 0.1 and  $b_2$  is set to be 0.12. Because of the waveform shape constraints in the time domain, for the designed optimal waveforms, there are still some powers allocated to the notched frequency band for two transmitter antennas. This amount of power can not be saved in order to keep the specific shapes of waveforms in the time domain. Meanwhile, all the spectral mask constraints and PAPR constraints are satisfied.

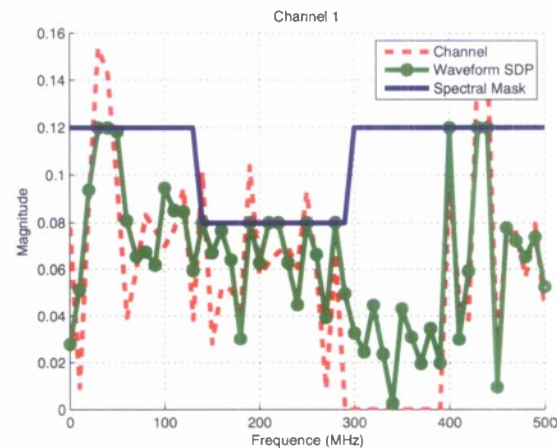


Figure 3.5: Designed waveform with PAPR consideration represented in frequency domain for channel 1.

Fig. 3.9 and Fig. 3.10 show designed optimal binary waveforms represented in frequency domain for two antennas respectively. Fig. 3.11 and Fig. 3.12 show designed optimal binary waveforms in correspondingly time domain for two antennas respectively. Fig. 3.13 shows the convergence of energy gaps between  $E_p$  and the dominant eigenvalue of  $\mathbf{P}^*$  with the number of iterations. When the dominant eigenvalue of  $\mathbf{P}^*$  approaches  $E_p$  very well, the optimal solution to the optimization problem (3.58) is obtained.

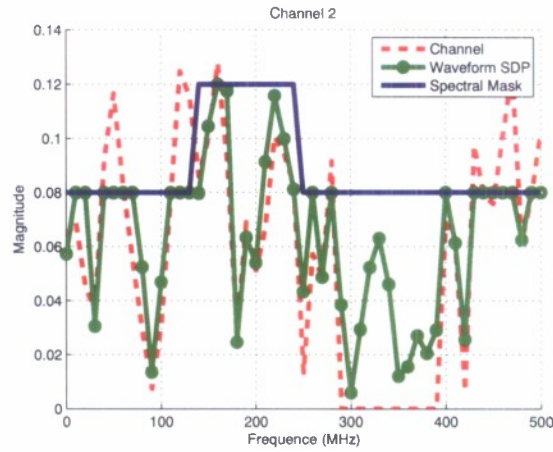


Figure 3.6: Designed waveform with PAPR consideration represented in frequency domain for channel 2.

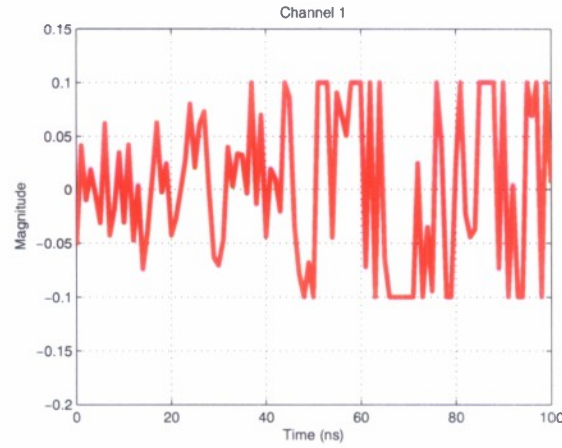


Figure 3.7: Designed waveform with PAPR consideration in time domain for channel 1.

### 3.1.6 Discussion

This section deals with wideband waveform optimization for MISO cognitive radio. Wideband waveforms are designed according to the optimization objective with the considerations of spectral mask constraint at the transmitter and the influence of arbitrary notch filter at the receiver. Meanwhile, PAPR and binary waveform design are also taken into account as the practical considerations in the context of MISO cognitive radio. The method of this section can be easily extended to the passband waveform design, where the individual oscillator for each antenna can be tied together to achieve coherency [8].

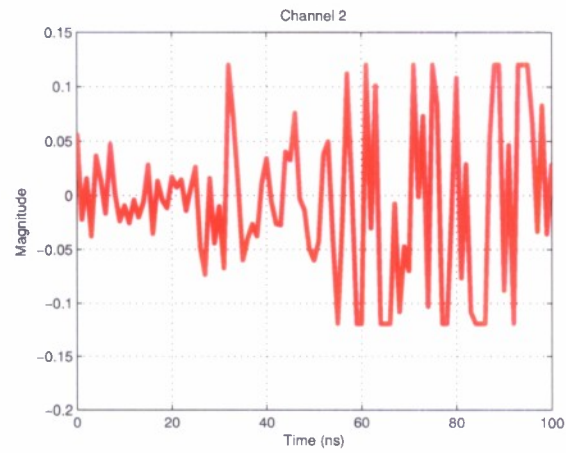


Figure 3.8: Designed waveform with PAPR consideration in time domain for channel 2.

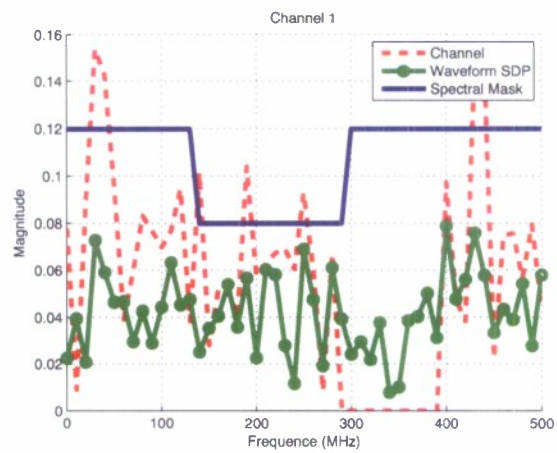


Figure 3.9: Designed binary waveform represented in frequency domain for channel 1.

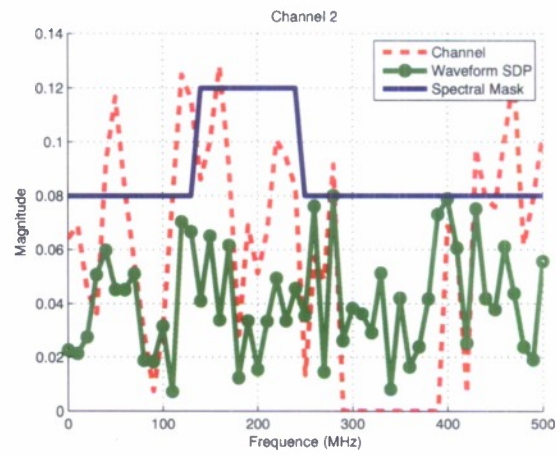


Figure 3.10: Designed binary waveform represented in frequency domain for channel 2.

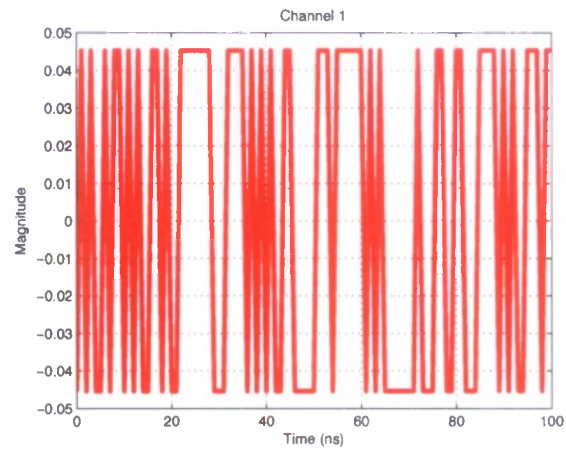


Figure 3.11: Designed binary waveform in time domain for channel 1.

### 3.1. WIDEBAND WAVEFORM OPTIMIZATION FOR MULTIPLE INPUT SINGLE OUTPUT COGNITIVE RADIO WI

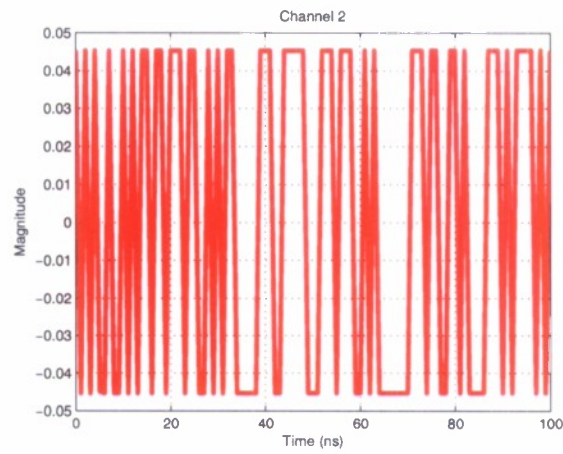


Figure 3.12: Designed binary waveform in time domain for channel 2.

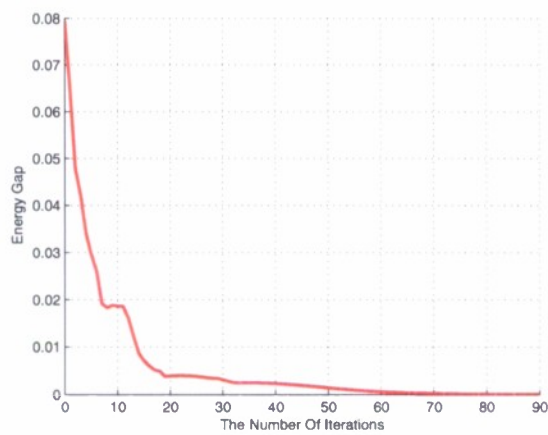


Figure 3.13: Energy gap.



## Bibliography

- [1] R. Qiu, C. Zhou, N. Guo, and J. Zhang, "Time reversal with miso for ultra-wideband communications: experimental results," in *Proc. IEEE Radio and Wireless Symposium*, pp. 499–502, 2006.
- [2] R. Q. N. Guo, J. Zhang and S. Mo., "Uwb miso time reversal with energy detector receiver over isse channels," in *4th Annual IEEE Consumer Communications and Networking Conference, Las Vegas, Nevada, USA*, 2007.
- [3] X. Li and M. Ismail, *Multi-Standard CMOS Wireless Receivers: Analysis and Design (The Springer International Series in Engineering and Computer Science)*. Springer, 2002.
- [4] N. Guo, J. Q. Zhang, P. Zhang, Z. Hu, Y. Song, and R. C. Qiu, "UWB Real-Time Testbed with Waveform-Based Precoding," in *IEEE Military Conference*, (San Diego, USA), November 2008.
- [5] N. Guo, Z. Hu, A. S. Saini, and R. C. Qiu, "Waveform-level Precoding with Simple Energy Detector Receiver for Wideband Communication," in *IEEE Southeastern Symposium on System Theory*, (Tulahoma, USA), March 2009.
- [6] Z. Hu, N. Guo, and R. C. Qiu, "Wideband Waveform Optimization for Energy Detector Receiver with Practical Considerations," in *IEEE International Conference on Ultra-Wideband*, (Vancouver, Canada), September 2009.
- [7] Z. Hu, N. Guo, and R. C. Qiu, "Wideband Waveform Optimization with Energy Detector Receiver in Cognitive Radio," in *IEEE Military Conference*, (Boston, USA), October 2009.
- [8] M. C. Wicks, "History of Waveform Diversity and Future Benefits to Military Systems." A Lecture Series on Waveform Diversity for Advanced Radar Systems, July 2009.
- [9] L. Vandenberghe and S. Boyd, "Semidefinite programming," *SIAM review*, vol. 38, no. 1, pp. 49–95, 1996.
- [10] D. Singh, Z. Hu, and R. C. Qiu, "UWB Channel Sounding and Channel Characteristics in Rectangular Metal Cavity," in *Proc of IEEE Southeastern Symposium*, (Huntsville, USA), April 2008.
- [11] R. C. Qiu, C. Zhou, J. Q. Zhang, and N. Guo, "Channel Reciprocity and Time-Reversed Propagation for Ultra-Wideband Communications," in *IEEE AP-S International Symposium on Antennas and Propagation*, 2007.
- [12] <http://www.stanford.edu/boyd/cvx/>.
- [13] S. Boyd and L. Vandenberghe, *Convex optimization*. Cambridge Univ Pr, 2004.